inorganics

MDPI

Article

Structurally Characterized Cobalt and Nickel Complexes of Flavonoid Chrysin as Potential Radical Scavenging Compounds

Eleftherios Halevas [1,2,*], Barbara Mavroidi [1], Despoina Varna [3], Georgia Zahariou [4], George Litsardakis [5], Maria Pelecanou [2] and Antonios G. Hatzidimitriou [3,*]

1 Institute of Biosciences & Applications, National Centre for Scientific Research "Demokritos", 15310 Athens, Greece; bmavroidi@bio.demokritos.gr
2 Laboratory of Biochemistry, Department of Chemistry, Aristotle University of Thessaloniki, 54124 Thessaloniki, Greece; pelmar@bio.demokritos.gr
3 Laboratory of Inorganic Chemistry, Department of Chemistry, Aristotle University of Thessaloniki, 54124 Thessaloniki, Greece; varndesp@chem.auth.gr
4 Institute of Nanoscience and Nanotechnology, National Centre for Scientific Research "Demokritos", 15310 Athens, Greece; zahariougeorgia@gmail.com
5 Laboratory of Materials for Electrotechnics, Department of Electrical and Computer Engineering, Aristotle University of Thessaloniki, 54124 Thessaloniki, Greece; lits@auth.gr
* Correspondence: lefterishalevas@gmail.com (E.H.); hatzidim@chem.auth.gr (A.G.H.); Tel.: +30-210-6503558 (E.H.); +30-2310-997748 (A.G.H.)

Abstract

Polyphenolic compounds, such as flavonoids, possess important structural and physico-chemical characteristics that in combination with their biological properties render them an important class of natural compounds with medicinal prospects. Chrysin is a well-known flavone with antioxidant activity and a multitude of other beneficial properties. The potential of flavonoids to coordinate with metal ions leads to derivatives with enhanced biological profile. Within this framework, four novel heteroleptic complexes of cobalt and nickel with chrysin and the aromatic bidentate chelating agents 2,2′-bipyridine and 1,10-phenanthroline were synthesized, as well as physico-chemically and structurally characterized. The *in vitro* antioxidant efficiency of the synthesized complexes was examined via the 2,2-diphenyl-1-picrylhydrazyl (DPPH) assay. All complexes showed notable radical scavenging capacity comparable to that of ascorbic acid, providing the incentive for further investigation of their therapeutic potential.

Keywords: cobalt and nickel complexes; flavonoid chrysin; antioxidant potential; radical scavenging activity

check for updates

Academic Editor: Dušan Dimić

Received: 10 June 2025
Revised: 2 July 2025
Accepted: 3 July 2025
Published: 7 July 2025

Citation: Halevas, E.; Mavroidi, B.; Varna, D.; Zahariou, G.; Litsardakis, G.; Pelecanou, M.; Hatzidimitriou, A.G. Structurally Characterized Cobalt and Nickel Complexes of Flavonoid Chrysin as Potential Radical Scavenging Compounds. *Inorganics* **2025**, *13*, 230. https://doi.org/10.3390/inorganics13070230

Copyright: © 2025 by the authors. Licensee MDPI, Basel, Switzerland. This article is an open access article distributed under the terms and conditions of the Creative Commons Attribution (CC BY) license (https://creativecommons.org/licenses/by/4.0/).

1. Introduction

Polyphenolic compounds, such as flavonoids, are the main components of several dietary supplements, fruits, plants, flowers, and medicinal herbs [1,2]. The presence of free hydroxyl moieties in their structure renders them beneficial in the management of oxidative stress, which accompanies many diseases. Further to the antioxidant properties [3], polyphenols possess significant biological activities including anticancer [4], antiallergic [5], anti-inflammatory [6], neuroprotective [7], and hepatoprotective ones [8], and, as a result, their impact in nutrition is constantly being upgraded. An important polyphenol with remarkable biological properties is the flavonoid chrysin (5,7-dihydroxyflavone), which has the flavone general structure with two hydroxyl groups at the 5 and 7 carbons of the A ring (Figure 1) [9]. Chrysin is copiously found in many plant extracts, as well as in propolis and

honey extracts [10,11]. It is also present in several medicinal plants and fruits, including *Passiflora caerulea* (blue passion flower), *Momordica charantia* (bitter melon) or *Pyrus pashia* (the wild Himalayan pear) [12,13].

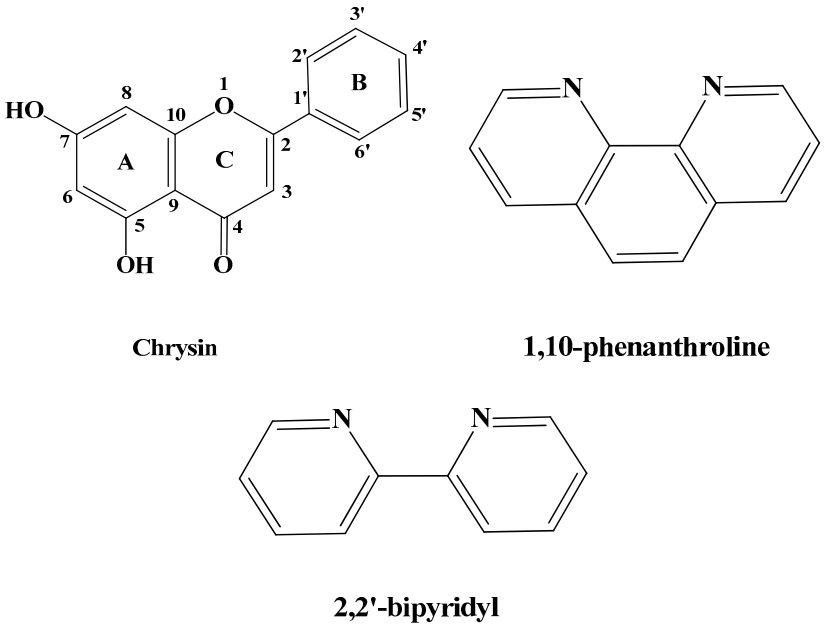


Figure 1. Schematic representation of the employed ligands chrysin (HL), 1,10-phenanthroline (phen) and 2,2′-bipyridyl (bpy).

Chrysin exhibits a well-investigated pharmacological profile. Further to its antioxidant and anti-inflammatory properties, chrysin has a well-established anti-cancer activity against a broad spectrum of cancers, including prostate, breast, lung, liver, colon and pancreatic cancer, and also human uveal melanoma, glioblastoma, and epidermoid carcinoma [14,15]. Furthermore, it has been welldocumented that the utilization of chrysin in applications of combination therapy enhances the efficiency of several chemotherapeutic drugs such as docetaxel [16], cisplatin, and camptothecin [17]. This can be explained by the intense interactions of chrysin metabolites with human serum albumins (HAS), affecting the albumin-binding properties and thus the biological activity, pharmacokinetics, and half-life of these drugs [18]. Moreover, chrysin has strong hepatoprotective effects protecting the liver cells from toxic substances [19], enhanced skin protective activity attenuating psoriasis-like skin lesions [20], significant neuroprotective properties improving memorization processes [21], and important antiviral activity against influenza H1N1 [22], coxsackie virus B3 (CVB3) [23], human rhinoviruses (HRV) [24], and others.

The bioactivity of chrysin is strongly related to its efficiency to interact with plasma proteins [18] and cell membranes [25], scavenge radicals [26], and chelate transition metal ions that produce radicals [27]. However, its fast metabolism, limited aqueous solubility, low systemic availability, and absorption rates have led researchers to develop metallochrysin complexes as substitute biologically active compounds with upgraded physicochemical and possibly, biological properties [13–15].

In our on-going research endeavors to generate innovative, bioactive metal complexes based on naturally derived chelators, the properties of chrysin were integrated with those of cobalt (Co) and nickel (Ni) metal ions. Ni is considered to be an important trace element for biological systems. Ni ions serve as enzyme cofactors of important enzymes including nickel superoxide dismutase, urease, carbon monoxide dehydrogenase, methyl-coenzyme M reductase, acetyl-coenzyme A synthase, acireductone dioxygenase, [NiFe]-hydrogenase, glyoxylase I and lactate racemase [28–30]. Furthermore, Ni(II) complexes display beneficial

activities, such as antimicrobial, antioxidant, anticancer, anticonvulsant, anti-inflammatory, and antileishmanial [31,32], while several Ni(II) complexes serve as DNA intercalators [33], cleaving agents [34], and potential binders to serum albumins [35]. On the other hand, Co is also a crucial trace element which shows interest, mainly due to its existence in the vitamin B12 active center. It can be found in both cobalamin-dependent enzymes and non-corrin cobalt-containing enzymes [36]. Several Co(II) and Co(III)-based metallo-complexes display remarkable antitumor, anti-angiogenic, antimicrobial, antiviral and antioxidant properties [37–40], and act as hydrolytic agents for DNA cleavage [41] and binding [42].

In light of the preceding facts, in this work we demonstrate the synthetic procedure, physico-chemical characterization, structural elucidation, and the DPPH radical scavenging activity of four novel Co(II), Co(III), and Ni(II) heteroleptic complexes with chrysin (HL) and the auxiliary *N*,*N*-donor ligands 1,10-phenanthroline (phen) and 2,2′-bipyridine (bpy) (Figure 1). Until today, there are no structurally elucidated, through single-crystal X-ray diffractometry, chrysin-based complexes of Co and Ni reported in the literature.

2. Results

2.1. Synthesis

A comprehensive examination of the reaction parameters including pH, temperature, metal-to-ligand-to-chelator molar ratios, solvent system, and crystallization procedures, led to the generation of heteroleptic Co(III)-chrysin-bpy, Co(II)-chrysin-phen, Ni(II)-chrysin-bpy, and Ni(II)-chrysin-phen complexes in alcoholic media and in sufficient yields. A detailed presentation of the examined reaction and (re)crystallization parameters and observations is presented in Supplementary Information Table S1. The stoichiometric equations that led to complexes **1**–**4** are presented in Scheme 1 below:

$$4\,[Co(NO_3)_2{\cdot}6H_2O] + 4\,HL + 8\,bpy + 6\,EtOH + O_2 \xrightarrow[Co^{+2} \rightarrow Co^{+3}]{N(C_2H_5)_3} 4\,\{[Co(L)(bpy)_2]{\cdot}(NO_3)_2{\cdot}1.5EtOH\} + 26\,H_2O$$

Complex 1

$$2\,Co(NO_3)_2{\cdot}6H_2O + 2\,HL + 2\,phen + 2\,N(C_2H_5)_3 + 6\,MeOH \longrightarrow [Co_2(L)_2(phen)_2(MeOH)_2]{\cdot}(NO_3)_2{\cdot}4MeOH + 2\,\{[(C_2H_5)_3NH](NO_3)\} + 12\,H_2O$$

Complex 2

$$2\,Ni(NO_3)_2{\cdot}6H_2O + 2\,HL + 2\,bpy + 2\,N(C_2H_5)_3 + 4\,EtOH \longrightarrow [Ni_2(L)_2(bpy)_2(EtOH)_2]{\cdot}(NO_3)_2{\cdot}2EtOH + 2\,\{[(C_2H_5)_3NH](NO_3)\} + 12\,H_2O$$

Complex 3

$$2\,Ni(NO_3)_2{\cdot}6H_2O + 2\,HL + 2\,phen + 2\,N(C_2H_5)_3 + 5\,EtOH \longrightarrow [Ni_2(L)_2(phen)_2(EtOH)_2]{\cdot}(NO_3)_2{\cdot}3EtOH + 2\,\{[(C_2H_5)_3NH](NO_3)\} + 12\,H_2O$$

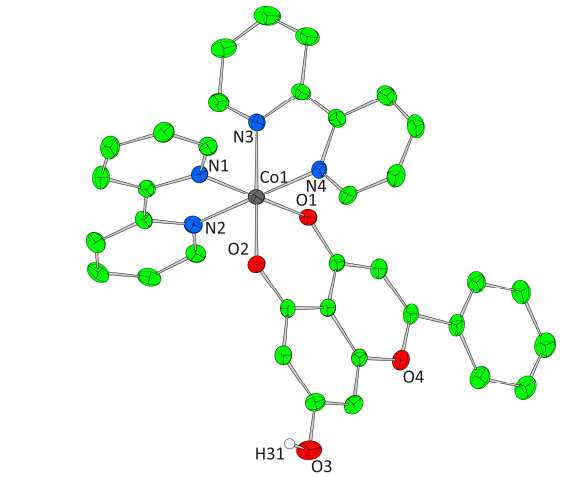
Complex 4

Scheme 1. Stoichiometric equations of complexes **1**–**4**.

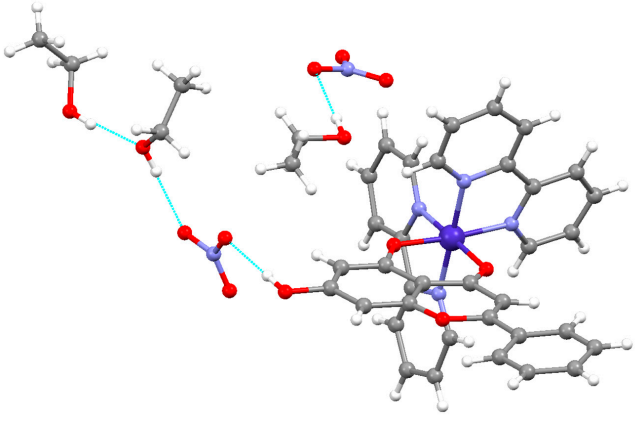
Ethanol was selected as the most adequate reaction solvent for the generation of stable crystalline materials in the cases of complexes **1**, **3**, and **4**. However, in the case of complex **2**, methanol was proved the most appropriate reaction solvent for the formation of a crystalline product of sufficient yield and with the ability to maintain its crystallinity right after its isolation from the mother liquor and for fairly long periods of time. Diethylether was employed as the precipitation inducing solvent to all the reaction solutions. Dark brown and dark red crystals emerged in the reactions of Co(III) and Co(II), respectively, whereas green crystals emerged in the case of Ni(II) reactions. The verification of the generated crystalline products was performed via elemental analysis, X-ray crystallography, and FT-IR spectroscopy. All materials retain their crystallinity when exposed to air and are insoluble in dichloromethane, acetone and acetonitrile, soluble in dimethylacetamide (DMA), dimethylsulfoxide (DMSO), dimethylformamide (DMF), MeOH and EtOH, and moderately soluble in H_2O under ambient conditions.

2.2. X-Ray Crystallographic Analysis

Figures 2A, 3A, 4A and 5A illustrate the solid-state lattices of **1**–**4**. The crystal collection data are given in Table 1, while the interatomic bond angles and lengths are provided in Table 2 [43–47]. In all cases, the monoionic chrysin is coordinated to the metal centers (Co(III), Co(II), and Ni(II)) in a bidentate mode via the deprotonated phenolic and carbonyl oxygens, leading to a six-membered ring rigid formation. In the case of the divalent metal ion complexes, the deprotonated phenolic oxygen is also acting as bridge between two metal centers forming a $M^{II}_2O_2$ four-membered ring.



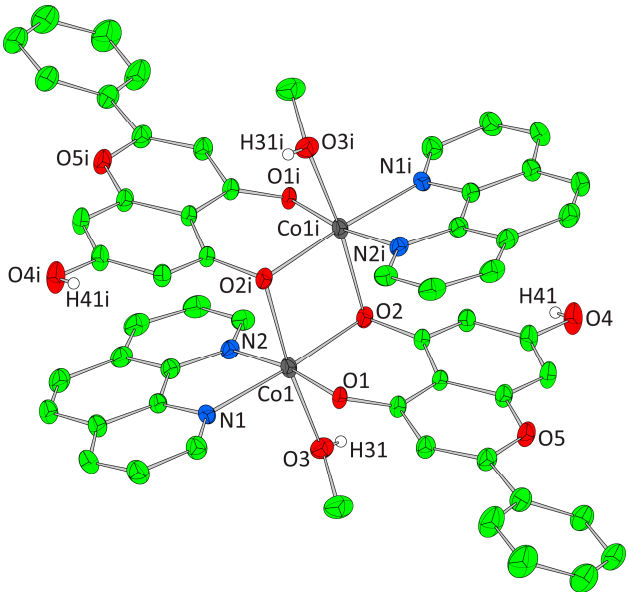
(**A**)



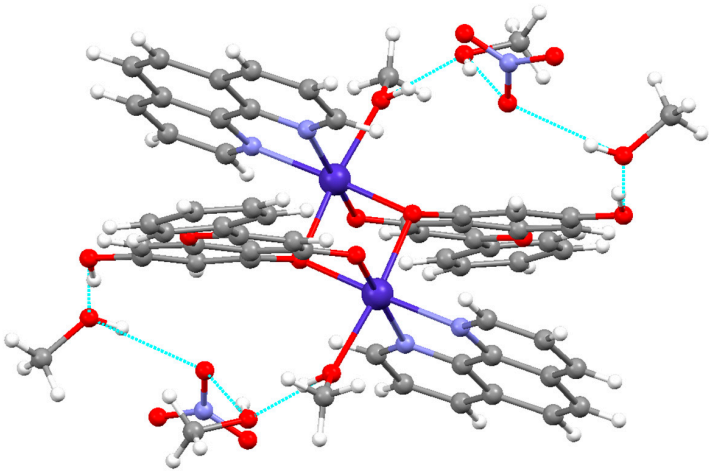
(**B**)

Figure 2. (**A**) Cameron scheme of $[Co(L)(bpy)_2]^{2+}$ complex assembly in compound **1**. Aromatic hydrogen atoms omitted for clarity. (**B**) Hydrogen bonding in complex **1** (light blue dotted lines).

Complex **1** crystallizes in the monoclinic space group $P2_1/n$ and its unit cell contains four molecules. The crystal asymmetric unit consists of two nitrate (NO_3^-) counter ions, one dicationic $[Co(L)(bpy)_2]^{2+}$ complex assembly, and one and a half lattice EtOH molecules. The molecular structure of **1** is composed of a Co(III) ion that is coordinated with one deprotonated chrysin and two bpy chelators, giving rise to a $Co^{III}N_4O_2$ chromophore with a distorted octahedral arrangement (Figure 2A). The lattice of **1** includes local intermolecular hydrogen bonds that are developed between the hydroxyl groups of the lattice EtOH molecules, the oxygens of the NO_3^- groups, and the non-coordinated phenolic group that derives from the deprotonated chrysin giving stability to the formed structure (Figure 2B, Supplementary Information Table S2).



(**A**)



(**B**)

Figure 3. (**A**) Cameron scheme of $[Co_2(L)_2(phen)_2(MeOH)_2]^{2+}$ complex assembly in compound **2**. Aromatic and methyl hydrogen atoms are omitted for clarity. (**B**) Hydrogen bonding in complex **2** (azure dotted lines).

Complex **2** crystallizes in the triclinic space group $P\bar{1}$ and its unit cell consists of four lattice MeOH molecules, one $[Co_2(L)_2(phen)_2(MeOH)_2]^{2+}$ cation, and two NO_3^- counter ions. Each Co(II) cation is bound to the oxygen of a MeOH molecule, two oxygens from

one monoanionic *O*,*O*-donor chrysin, two nitrogen atoms of one phen molecule as well as the bridging deprotonated phenolic oxygen of a second chrysin from the symmetrically developed neighboring $[Co(L)(phen)(MeOH)]^+$ formation. Thus, the final dimer dinuclear complex dication is formed. Each metal center presents a $Co^{II}N_2O_4$ chromophore and a coordination arrangement with a distorted octahedral geometry (Figure 3A). The lattice of **2** includes four intermolecular hydrogen bonding interactions. The unbound phenolic oxygens of chrysin ligands bind to the oxygen of a lattice MeOH molecule. The oxygen atom of the ligated MeOH molecule binds the oxygen of the second lattice MeOH molecule. Finally, both oxygen atoms of the two lattice MeOH molecules bind the same oxygen of the NO_3^- anion thus forming a local network of hydrogen bonding interactions giving further stability to the lattice formed (Figure 3B, Supplementary Information Table S2).

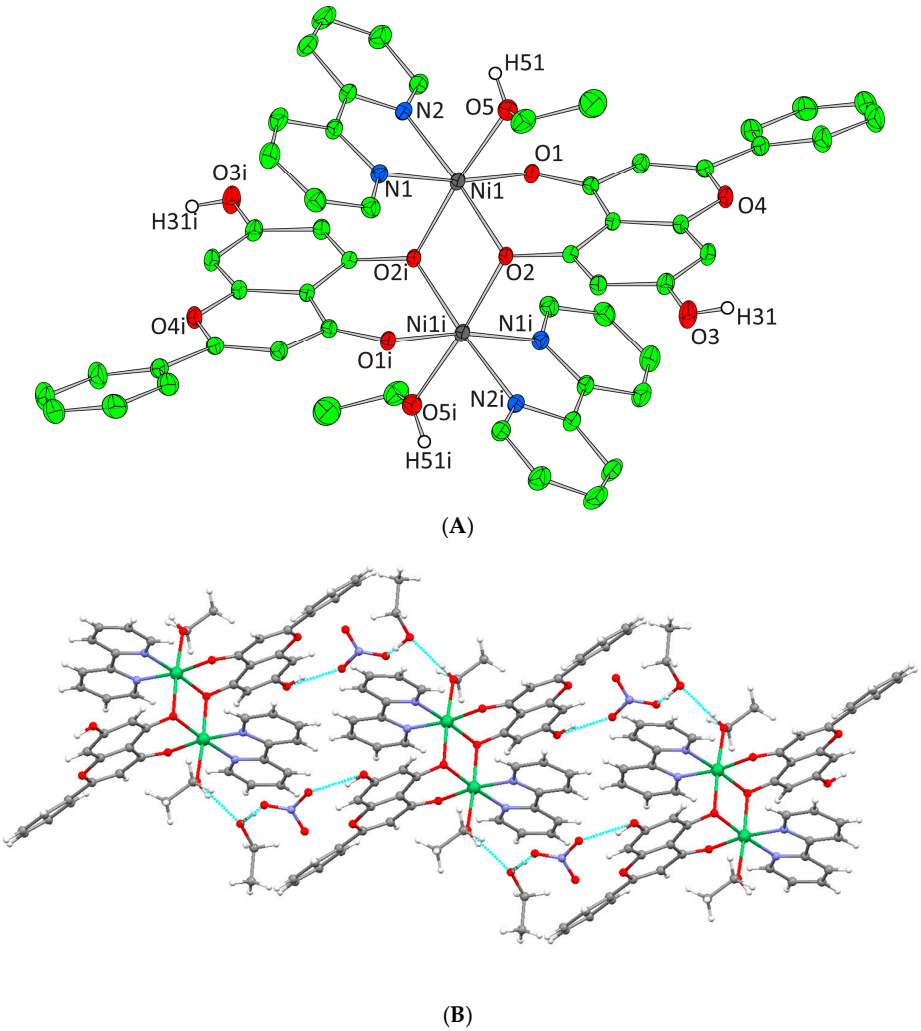
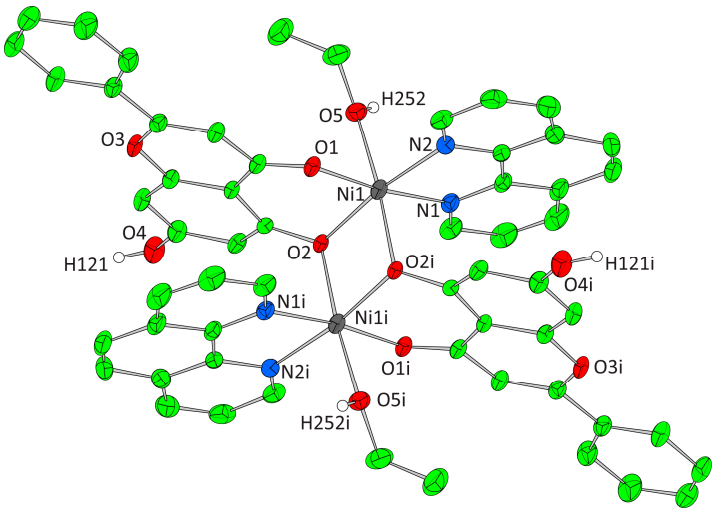


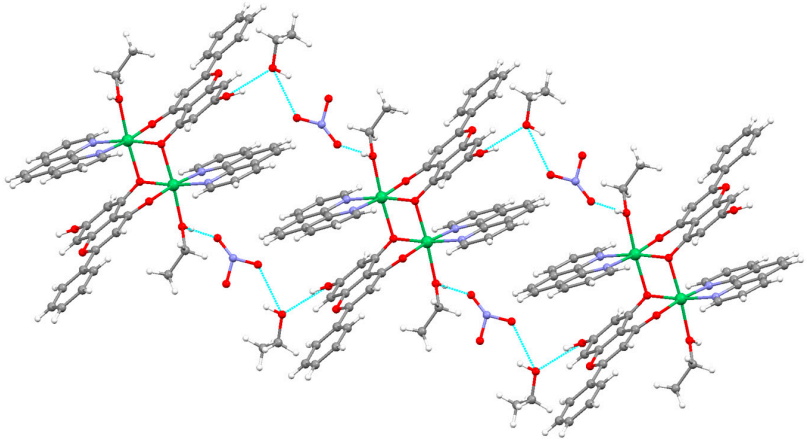
Figure 4. (**A**) Cameron scheme of $[Ni_2(L)_2(bpy)_2(EtOH)_2]^{2+}$ complex assembly in compound **3**. Aromatic and ethyl hydrogen atoms are omitted for clarity. (**B**) Hydrogen bonding in complex **3** (azure dotted lines).

Complexes **3** and **4** crystallize in the triclinic space group *P*-1. The unit cell of **3** contains two lattice EtOH molecules, two NO_3^- counter ions, and one $[Ni_2(L)_2(bpy)_2(EtOH)_2]^{2+}$ cation. In the case of **4**, the unit cell contains three EtOH molecules, one $[Ni_2(L)_2(phen)_2(EtOH)_2]^{2+}$ cation, and two NO_3^- counter ions. Both binuclear complexes result from the dimerism of the mononuclear complex $[Ni(L)(N,N\text{-donor})(EtOH)]^+$, present in the asymmetric unit, as to the center of symmetry located on the center of Ni-Ni mid distance. The deprotonated phenolic oxygen atoms are acting not only as chelators for each metal

ion but also as bridges between them. Moreover, in both complexes, each Ni(II) ion is coordinated to one EtOH molecule, one monoionic chrysin, one bpy or phen molecule and the deprotonated phenolic oxygen of a second flavonoid molecule from the symmetrically developed assembly, giving rise to a $Ni^{II}N_2O_4$ chromophore around each Ni(II) core and a coordination arrangement with a distorted octahedral geometry (Figures 4A and 5A). Hydrogen bonding interactions in **3** and **4** emerge between the ligated ethanolic oxygen atom to one oxygen atom of a lattice NO_3^- anion while a second oxygen from the same NO_3^- anion interacts with the oxygen of a lattice EtOH. The latter also binds the free phenolic oxygen of a neighboring complex assembly thus forming a polymeric chain of hydrogen bonding interactions giving extra stability to the system and forming an extended final 1D crystal lattice (Figures 4B and 5B, Supplementary Information Table S2).



(**A**)



(**B**)

Figure 5. (**A**) Cameron plot of $[Ni_2(L)_2(phen)_2(EtOH)_2]^{2+}$ complex assembly in compound **4**. Aromatic and ethyl hydrogen atoms are omitted for clarity. (**B**) Hydrogen bonding in complex **4** (azure dotted lines).

The Co(III)-N (bpy), Co(III)-O, Co(II)-N (phen), Co(II)-O, Ni(II)-N (bpy), Ni(II)-N (phen) and Ni(II)-O bond lengths are in the range of 1.9099(19)–1.950(2) Å, 1.8445(17)–1.8806(16) Å, 2.101(2)–2.115(2) Å, 2.034(2)–2.147(2) Å, 2.043(2)–2.061(2) Å, 2.0067(19)–2.145(2) Å, 2.039(3)–2.076(3) Å, and 1.998(2)–2.137(2) Å, respectively. The measured lengths are similar to others found in literature reported Co(III), Co(II), and Ni(II) complexes [33,38,48].

Table 1. Summary of crystal, intensity collection and refinement data for $[Co(L)(bpy)_2]\cdot(NO_3)_2\cdot1.5(EtOH)$ (**1**), $[Co_2(L)_2(phen)_2](NO_3)_2\cdot2(MeOH)$ (**2**), $[Ni_2(L)_2(bpy)_2(EtOH)_2](NO_3)_2\cdot2(EtOH)$ (**3**), and $[Ni_2(L)_2(phen)_2(EtOH)_2](NO_3)_2\cdot3(EtOH)$ (**4**), where L is the deprotonated ligand chrysin.

Crystal Data				
	1	**2**	**3**	**4**
Chemical formula sum	$C_{38}H_{34}N_6O_{11.5}Co$	$C_{60}H_{58}N_6O_{20}Co_2$	$C_{58}H_{58}N_6O_{18}Ni_2$	$C_{64}H_{64}N_6O_{19}Ni_2$
Chemical formula moiety	$[Co(L)(bpy)_2]\cdot(NO_3)_2\cdot1.5(EtOH)$	$[Co_2(L)_2(phen)_2](NO_3)_2\cdot2(MeOH)$	$[Ni_2(L)_2(bpy)_2(EtOH)_2](NO_3)_2\cdot2(EtOH)$	$[Ni_2(L)_2(phen)_2(EtOH)_2](NO_3)_2\cdot3(EtOH)$
M_r	817.65	1301.01	1244.55	1338.66
Crystal system, Space group	Monoclinic, $P2_1/n$	Triclinic, *P*-1	Triclinic, *P*-1	Triclinic, *P*-1
Temperature (K)	295	295	295	295
a, b, c (Å)	13.144 (2), 10.9453 (17), 29.641 (5)	10.4626 (6), 11.2633 (8), 13.5977 (10)	10.6335 (12), 11.3275 (10), 13.8952 (17)	9.3331 (8), 12.6102 (12), 15.3374 (12)
a (°) β (°) γ (°)	98.340 (5)	87.743 (4) 71.447 (3) 76.325 (3)	72.933 (6) 71.685 (6) 66.191 (5)	72.730 (4) 88.713 (4) 68.463 (4)
V (Å^3)	4219.3 (12)	1474.94 (18)	1426.7 (3)	1595.7 (2)
Z	4	1	1	1
Radiation type	Mo Kα	Mo Kα	Mo Kα	Mo Kα
μ (mm^{-1})	0.47	0.65	0.74	0.67
Crystal size (mm)	0.23 × 0.16 × 0.15	0.25 × 0.23 × 0.15	0.15 × 0.07 × 0.06	0.19 × 0.18 × 0.12
Data collection				
Diffractometer	Bruker Kappa Apex2	Bruker Kappa Apex2	Bruker Kappa Apex2	Bruker Kappa Apex2
Absorption correction	Numerical Analytical Absorption [49]	Numerical Analytical Absorption [49]	Numerical Analytical Absorption [49]	Numerical Analytical Absorption [49]
Tmin, Tmax	0.93, 0.93	0.86, 0.91	0.95, 0.96	0.89, 0.92
No. of measured, independent and observed [I > 2.0σ(I)] reflections	41,491, 7992, 5795	19,214, 5549, 4560	17,025, 5406, 3980	27,053, 6093, 4366
Rint	0.028	0.021	0.023	0.030
(sin θ/λ)max (Å^{-1})	0.613	0.613	0.615	0.613
Refinement				
R[F^2 > 2σ(F^2)], wR(F^2), S	0.048, 0.087, 1.00	0.046, 0.091, 1.00	0.039, 0.077, 1.00	0.044, 0.084, 1.00
No. of reflections	5795	4560	3980	4366
No. of parameters	505	397	373	413
No. of restraints	6	0	12	10
H-atom treatment	H-atom parameters constrained	H-atom parameters constrained	H-atom parameters constrained	H atoms treated by a mixture of independent and constrained refinement
$\Delta\rho_{max}, \Delta\rho_{min}$ (e Å^{-3})	0.33, −0.48	0.35, −0.90	0.60, −0.49	0.48, −0.30

Table 2. Bond lengths [Å] and angles [deg] for $[Co(L)(bpy)_2]\cdot(NO_3)_2\cdot 1.5(EtOH)$ (**1**), $[Co_2(L)_2(phen)_2](NO_3)_2\cdot 2(MeOH)$ (**2**), $[Ni_2(L)_2(bpy)_2(EtOH)_2](NO_3)_2\cdot 2(EtOH)$ (**3**), and $[Ni_2(L)_2(phen)_2(EtOH)_2](NO_3)_2\cdot 3(EtOH)$ (**4**), where L is the deprotonated ligand chrysin.

Bond Lengths (Å)							
1		**2**		**3**		**4**	
Co(1)—O(1)	1.8806 (16)	Co(1)—O(2)^{i}	2.137 (2)	Ni(1)—O(2)^{i}	2.112 (2)	Ni(1)—O(2)^{i}	2.137 (2)
Co(1)—O(2)	1.8445 (17)	Co(1)—N(1)	2.101 (2)	Ni(1)—O(1)	2.0067 (19)	Ni(1)—O(1)	2.0123 (19)
Co(1)—N(1)	1.9099 (19)	Co(1)—N(2)	2.115 (2)	Ni(1)—O(2)	2.0098 (19)	Ni(1)—O(2)	1.998 (2)
Co(1)—N(2)	1.923 (2)	Co(1)—O(1)	2.0492 (19)	Ni(1)—O(5)	2.145 (2)	Ni(1)—O(5)	2.125 (2)
Co(1)—N(3)	1.950 (2)	Co(1)—O(2)	2.034 (2)	Ni(1)—N(1)	2.061 (2)	Ni(1)—N(1)	2.076 (3)
Co(1)—N(4)	1.925 (2)	Co(1)—O(3)	2.147 (2)	Ni(1)—N(2)	2.043 (2)	Ni(1)—N(2)	2.039 (3)
Angles (°)							
1		**2**		**3**		**4**	
O(1)—Co(1)—O(2)	96.70 (7)	O(2)^{i}—Co(1)—N(1)	96.05 (9)	O(2)^{i}—Ni(1)—O(1)	91.97 (8)	O(2)^{i}—Ni(1)—O(1)	90.25 (8)
O(1)—Co(1)—N(1)	175.32 (8)	O(2)^{i}—Co(1)—N(2)	89.76 (8)	O(2)^{i}—Ni(1)—O(2)	82.41 (8)	O(2)^{i}—Ni(1)—O(2)	82.11 (8)
O(2)—Co(1)—N(1)	86.26 (8)	N(1)—Co(1)—N(2)	79.18 (9)	O(1)—Ni(1)—O(2)	88.60 (8)	O(1)—Ni(1)—O(2)	88.72 (8)
O(1)—Co(1)—N(2)	93.47 (9)	O(2)^{i}—Co(1)—O(1)	95.81 (8)	O(2)^{i}—Ni(1)—O(5)	175.16 (8)	O(2)^{i}—Ni(1)—O(5)	175.52 (9)
O(2)—Co(1)—N(2)	87.33 (8)	N(1)—Co(1)—O(1)	94.19 (8)	O(1)—Ni(1)—O(5)	87.11 (8)	O(1)—Ni(1)—O(5)	87.80 (9)
N(1)—Co(1)—N(2)	83.03 (9)	N(2)—Co(1)—O(1)	171.78 (9)	O(2)—Ni(1)—O(5)	92.81 (8)	O(2)—Ni(1)—O(5)	93.81 (9)
O(1)—Co(1)—N(3)	86.90 (8)	O(2)^{i}—Co(1)—O(2)	80.82 (8)	O(2)^{i}—Ni(1)—N(1)	93.46 (9)	O(2)^{i}—Ni(1)—N(1)	94.88 (9)
O(2)—Co(1)—N(3)	174.66 (8)	N(1)—Co(1)—O(2)	176.29 (9)	O(1)—Ni(1)—N(1)	170.80 (9)	O(1)—Ni(1)—N(1)	173.61 (10)
N(1)—Co(1)—N(3)	90.41 (9)	N(2)—Co(1)—O(2)	98.74 (9)	O(2)—Ni(1)—N(1)	99.47 (9)	O(2)—Ni(1)—N(1)	95.74 (9)
N(2)—Co(1)—N(3)	96.42 (9)	O(1)—Co(1)—O(2)	88.13 (8)	O(5)—Ni(1)—N(1)	88.08 (9)	O(5)—Ni(1)—N(1)	87.35 (10)
O(1)—Co(1)—N(4)	86.96 (8)	O(2)^{i}—Co(1)—O(3)	170.87 (8)	O(2)^{i}—Ni(1)—N(2)	93.21 (9)	O(2)^{i}—Ni(1)—N(2)	91.29 (9)
O(2)—Co(1)—N(4)	92.14 (9)	N(1)—Co(1)—O(3)	91.92 (9)	O(1)—Ni(1)—N(2)	92.56 (9)	O(1)—Ni(1)—N(2)	95.48 (10)
N(1)—Co(1)—N(4)	96.58 (9)	N(2)—Co(1)—O(3)	87.37 (9)	O(2)—Ni(1)—N(2)	175.50 (10)	O(2)—Ni(1)—N(2)	172.21 (9)
N(2)—Co(1)—N(4)	179.35 (9)	O(1)—Co(1)—O(3)	88.01 (8)	O(5)—Ni(1)—N(2)	91.59 (10)	O(5)—Ni(1)—N(2)	92.91 (10)
N(3)—Co(1)—N(4)	84.09 (9)	O(2)—Co(1)—O(3)	91.05 (8)	N(1)—Ni(1)—N(2)	79.73 (10)	N(1)—Ni(1)—N(2)	80.62 (11)
				Ni(1)^{i}—O(2)—Ni(1)	97.59 (8)	Ni(1)^{i}—O(2)—Ni(1)	97.89 (8)

Symmetry code: (i) −x+1, −y+1, −z+1.

2.3. FT-IR Studies

The FT-IR spectroscopy data were in agreement with the structure of complexes **1–4** and display significant modifications of vibrational patterns of the ligands upon metal ion complexation (Supplementary Information Figure S2). In the free chrysin spectrum, an intense band was observed at 1652 cm^{-1}, demonstrating the C=O bond stretching vibration of the chromone ring. The strong signals at 1448 cm^{-1}, 1575 cm^{-1} and 1608 cm^{-1} are indicative of the ν(C=C) stretching in the γ-pyrone and benzene rings. The δ(O–H) and ν(C−O) linked vibrational modes are spotted at 1312 cm^{-1} and 1354 cm^{-1}, respectively. The v(C–O–C) stretching signals are spotted at 1244 cm^{-1}, whereas the phenolic stretches ν(C–H) and v(O–H) are detected between 2627 cm^{-1} and 3150 cm^{-1} [50,51].

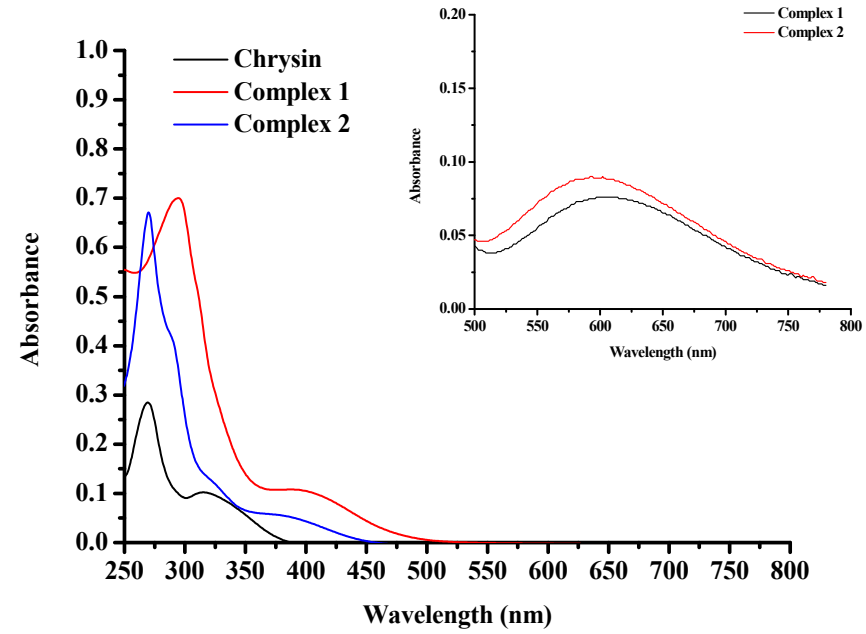
In the spectra of the complex assemblies, the intense signals at 1632 cm^{-1} for **1**, 1629 cm^{-1} for **2**, 1625 cm^{-1} for **3** and 1629 cm^{-1} for **4**, are indicative of the v(C=O) stretches and exhibit a shift to lower energy in comparison to plain flavonoid, in agreement with coordination to the metal cores [50,51]. The bands at 1312 cm^{-1} and 1338 cm^{-1} for **1**, 1279 cm^{-1} and 1325 cm^{-1} for **2**, 1266 cm^{-1} and 1302 cm^{-1} for **3** and 1280 cm^{-1} and 1324 cm^{-1} for **4**, indicative of the coupled ν(C–O) and δ(O–H) vibrations, show notable shifts to lower energy in comparison to plain chrysin. The bands located at 1402 cm^{-1} for **1**, 1386 cm^{-1} for **2**, 1354 cm^{-1} for **3** and 1404 cm^{-1} for **4**, are due to the degenerate $\nu 3(E')$ stretches of the planar (*D3h*) NO^{3-} anion [52]. In all complexes, the weak but distinguishable bands in the 3100–2800 cm^{-1} region, are due to the v(O–H) and aromatic v(*C–H*) stretches. The bands at 1243 cm^{-1} for **1**, 1279 cm^{-1} for **2**, 1266 cm^{-1} for **3** and 1245 cm^{-1} for **4**, are attributed to the v(C–O–C) vibrational modes. The signals located at 574 cm^{-1} for **1**, 562 cm^{-1} for **2**, 559 cm^{-1} for **3** and 652 cm^{-1} for **4**, can be attributed to the v(M–O) stretches [53].

In the spectra of **1** and **3**, the v(C–N) stretches indicating the bpy moiety, can be spotted at 1520 cm^{-1} and 1538 cm^{-1}, respectively, exhibiting shifts to lower frequencies due to the coordination to the metal ions [54]. A similar observation applies for the stretches of the phen molecule in the spectra of **2** and **4** that can be found at around 1538 cm^{-1}. The indicative out-of-plane C–H deformation motion on the heterocyclic rings can be found as strong bands between 832–728 cm^{-1} for **1**, 860–726 cm^{-1} for **2**, 864–735 cm^{-1} for **3** and 862–725 cm^{-1} for **4**, respectively [54].

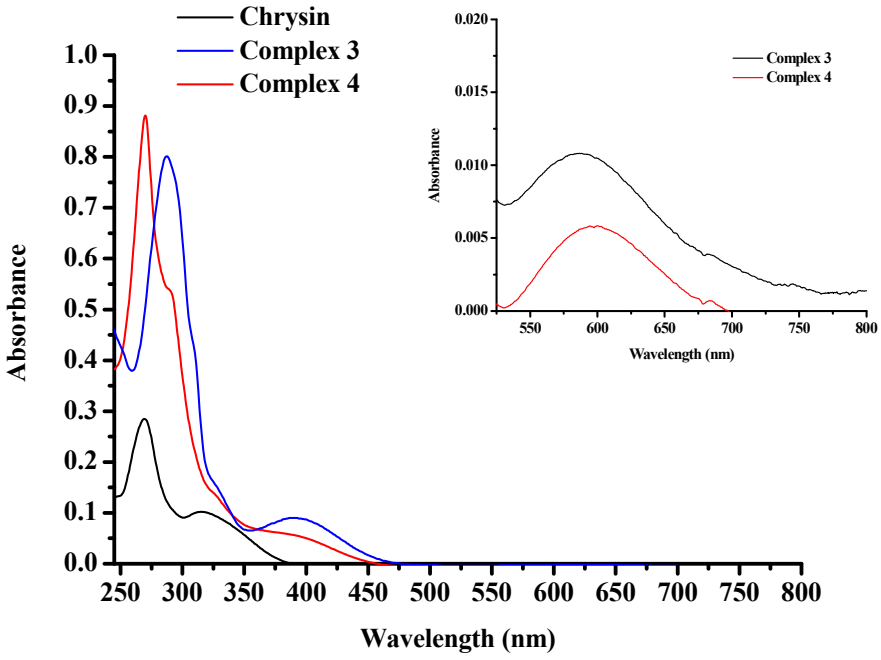
2.4. UV-Vis Studies

The UV–Vis spectra of pure chrysin, **1** and **2** (Figure 6A), as well as **3** and **4** (Figure 6B), were recorded in EtOH (10^{-5} M). The chrysin spectrum demonstrates a high intensity absorption signal at 270 nm (ε~28,490 $M^{-1}{\cdot}cm^{-1}$), characteristic of the $\pi \rightarrow \pi^*$ electronic transitions over Band II (A and C rings), and a broader lower signal around 315 nm, indicative of $\pi \rightarrow \pi^*$ transitions over Band I (B-ring) [50,51]. The UV-Vis spectra of **1–4** display an intense hyperchromic shift of the Band II maximum absorption compared to pure flavonoid. A strong shift of this band to longer wavelengths (315 nm) was observed in the spectra of **1** and **3**. These shifts are characteristic of the rigid flavonoid coordination to the metal core in combination with ligand-to-metal charge transfer (LMCT) interactions [50–52,55]. More accurately, Band II shows up at 295 nm (ε~70,030 $M^{-1}{\cdot}cm^{-1}$) for **1** and at 287 nm (ε~80,100 $M^{-1}{\cdot}cm^{-1}$) for **3**, showing shifts of 25 nm and 17 nm, respectively, compared to pure flavonoid, and at 270 nm for **2** (ε~67,141 $M^{-1}{\cdot}cm^{-1}$) and **4** (ε~88,138 $M^{-1}{\cdot}cm^{-1}$). Band I can be observed as a very weak shoulder in the spectrum of complexes **2**, **3** and **4** at around 328 nm, confirming the absence of B ring from the complexation process. The broad bands at around 395 nm (ε~10,979 $M^{-1}{\cdot}cm^{-1}$) for **1**, 380 nm (ε~6010 $M^{-1}{\cdot}cm^{-1}$) for **2**, 389 nm for **3** (ε~9000 $M^{-1}{\cdot}cm^{-1}$) and 388 nm for **4** (ε~5952 $M^{-1}{\cdot}cm^{-1}$) can be assigned to the LMCT process [50–52,55]. A weak shoulder observed at around 289 nm

(ε~42,640 $M^{-1} \cdot cm^{-1}$) for complexes **2** and **4** is due to the $\pi \rightarrow \pi^*$ charge transfer of the chelated phen molecule [56]. Nevertheless, in the spectra of complexes **1** and **3**, a similar signal cannot be easily distinguished.



(**A**)



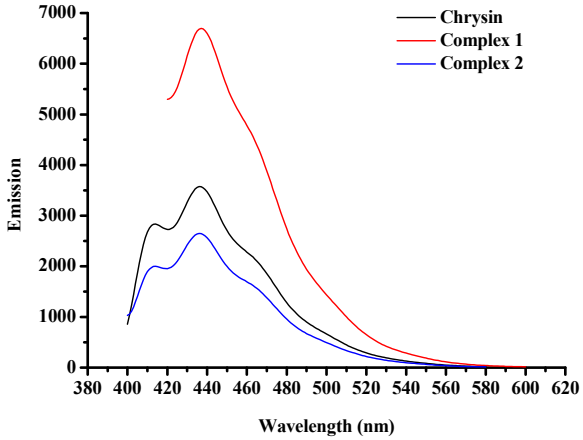
(**B**)

Figure 6. UV-Vis spectra of (**A**) **1** (red line), **2** (blue line), and pure chrysin (black line); and (**B**) **3** (blue line), **4** (red line), and plain chrysin (black line), in EtOH at 10^{-5} M. The inset graphs in both spectra present the d–d transitions detected in EtOH at 10^{-3} M.

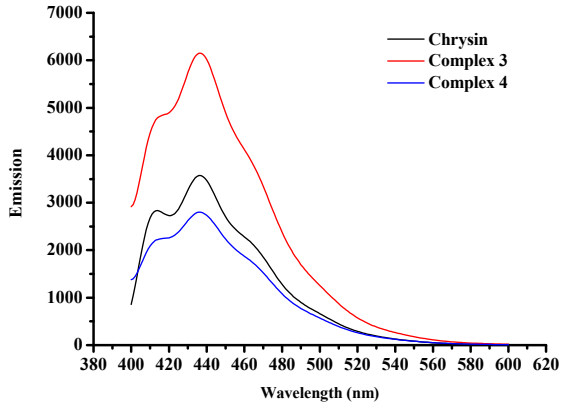
No d–d transitions are detected in the spectra of complexes **1–4** due to the low concentration of the solutions (10^{-5} M). Additional measurements at 10^{-3} M showed broad bands at 606 nm for **1**, 593 nm for **2**, 584 nm for **3** and 597 for **4**, respectively, characteristic of d–d transitions (Figure 6A, B inset graphs).

2.5. Fluorescence Studies

Emission spectra of the free flavonoid and complexes **1**–**4** were measured in EtOH solutions (10^{-5} M), at ambient temperature (Figure 7A, B). In particular, chrysin in its free form exhibits two emission bands with emission maxima at 414 and 436 nm, upon excitation at 270 nm. Complexes **1** and **3** show emission maxima at 437 and 436 nm, respectively, when excited at 295 nm. An additional emission band of lower intensity was observed at 414 nm, in the spectrum of **3**. Emission spectra of **2** and **4** show reduced emission maxima in comparison to plain chrysin whereas complexes **1** and **3** present enhanced emission. Complex **2** displays an emission maximum at 436 nm and a weaker signal at 413 nm whereas for complex **4**, the corresponding signals are observed at 436 and 415 nm, upon excitation at 270 nm. The intensity variations of the emission signals of **1**–**4** compared to the plain flavonoid may reflect the rigidity of coordination of chrysin to the metal cores [50–52]. In general, the emission at higher energies is attributed to the contribution of chrysin in the fluorescence of the complexes. However, at lower energies all complexes exhibit emission maxima that are assigned to the d–d transitions in the metal center. Due to the presence of potential aggregates in solution that may lead to decrease of fluorescence, the emission spectra at 600–800 nm were recorded in solid state and are presented in Supplementary Information Figure S3. The corresponding excitation spectra of complexes **1**–**4** are presented in Supplementary Information Figure S4. Table 3 summarizes the emission band maxima λ_{max}(em) (nm) in EtOH solutions (10^{-5} M) and solid state.



(**A**)



(**B**)

Figure 7. Fluorescence spectra of (**A**) pure chrysin, **1**, and **2**, and (**B**) pure chrysin, **3**, and **4**, in EtOH at a concentration of 10^{-5} M.

Table 3. Emission band maxima λ_{max}(em) (nm) in EtOH solutions (10^{-5} M) and solid state.

Complex	λ_{max}(em)/(nm)
1	437, 649, 752
2	436, 649, 752
3	436, 708, 748
4	415, 436, 708, 748

2.6. Thermogravimetric Studies

The thermal degradation of complexes **1**–**4** was assessed via thermogravimetric analysis (TGA), in air (Figure 8A,B).

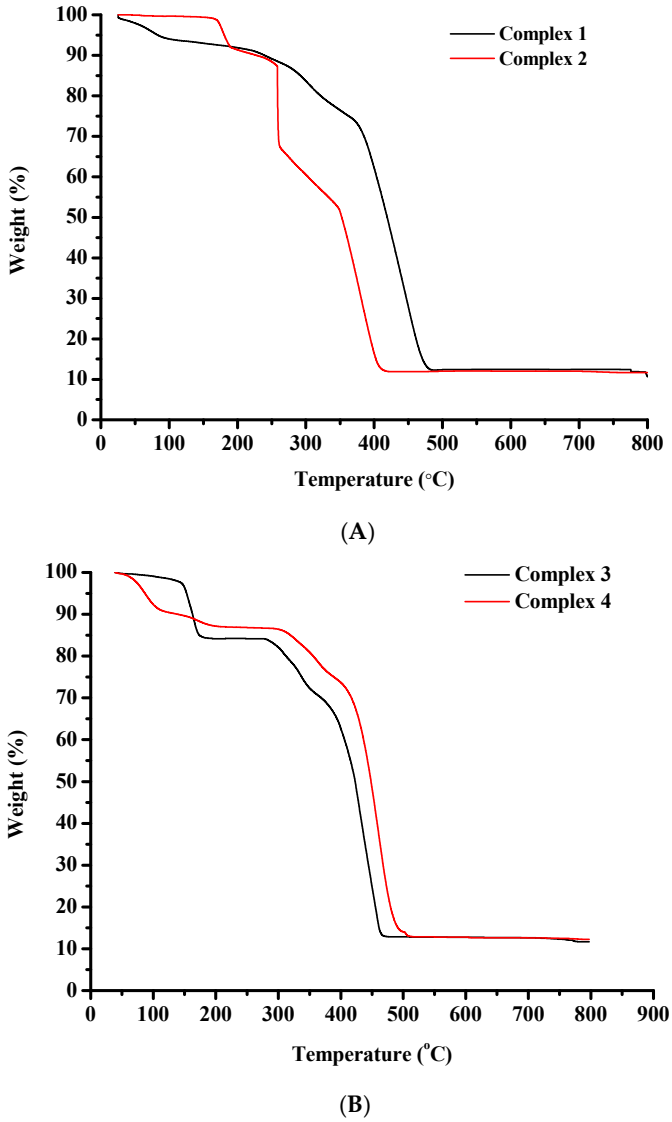


Figure 8. TGA diagrams of (**A**) complexes **1** and **2,** and (**B**) complexes **3** and **4**.

The thermal decomposition of complex **1** begins at 25 °C and proceeds rapidly until 100 °C potentially due to the discharge of volatile compounds. Between 100 °C and 215 °C the rate decreases. After 215 °C and until 485 °C the decomposition curve descends very rapidly and a significant weight loss can be observed that could be attributed to the destruction of the organic constituents of the starting molecule. A horizontal portion is located between 485 °C and 800 °C.

Complex **2** is thermally stable until 165 °C. From this point a rapid weight loss is detected that may be attributed to the degradation of the organic matter of the starting molecule. The curve descends continuously accompanied by abrupt changes in direction until 422 °C. A perfectly horizontal portion is spotted between 422 °C and 800 °C.

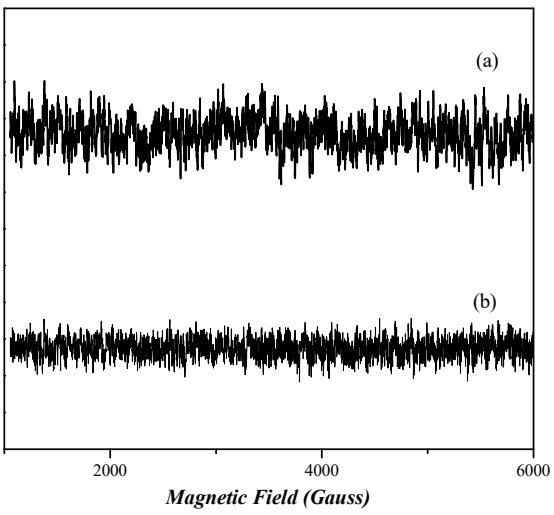
A negligible weight loss is noticed for complex **3** between 25 °C and 145 °C indicative of the release of volatile substances. From this point on, a rapid weight loss is noticed until 185 °C. After that, a horizontal portion of the decomposition curve is recorded between 185 °C and 277 °C. The decomposition then proceeds very rapidly up to 475 °C pointing to the destruction of the organic constituents of the starting molecule. Subsequently, a plateau appears that remains stable until 800 °C.

The thermal decomposition of complex **4** begins at 25 °C and proceeds rapidly until 205 °C, potentially due to the release of volatile substances. After that, a horizontal portion of the decomposition curve is located between 205 °C and 290 °C. Then the complex decomposes very rapidly until 510 °C pointing to the destruction of the organic substances of the starting molecule. Subsequently, a horizontal portion appears and remains until 800 °C.

The performed analysis is consistent with documented TGA data on Co(II), Co(III) and Ni(II)-containing compounds [57].

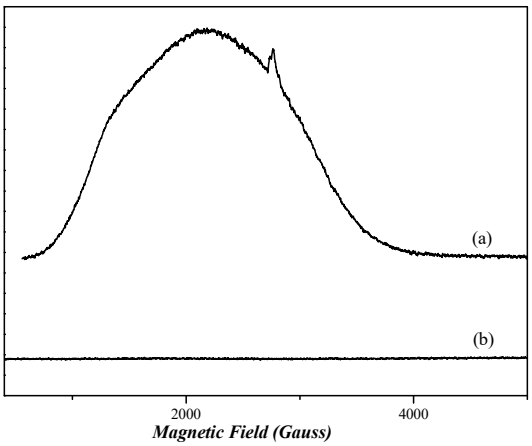
2.7. EPR Analysis

The continuous wave (cw) X-band EPR spectra [58] of frozen dimethyl sulfoxide (DMSO) solutions of nickel complexes **3** and **4** in are depicted in Figure 9A. The spectra of both complexes do not present any EPR signal, indicating that both compounds are diamagnetic. Figure 9B shows the X-band EPR spectra of cobalt complexes **1** and **2**. The spectrum of complex **1** presents a very wide EPR signal which indicates the paramagnetic nature of this compound. However, the determination of the spin value is impossible, due to the broadness of the EPR signal. In the case of complex **2**, the absence of an EPR signal indicates that it is diamagnetic.



(**A**)

Figure 9. *Cont.*



(**B**)

Figure 9. CW X-band EPR spectra of complexes **1**, **2**, **3**, and **4**, all diluted in DMSO at ~1 mM. (**A**) Complex **4** (trace a) and complex **3** (trace b). (**B**) Complex **1** (trace a) and complex **2** (trace b). Measurement conditions: T = 6 K, modulation amplitude 12.5 Gpp, microwave frequency 9.41 GHz, microwave power 30 mW.

2.8. Antioxidant Activity

The antioxidant activity of complexes **1**–**4** was determined *in vitro* through their potential to scavenge free DPPH radicals [59] and is depicted in Figure 10. The well-known antioxidant ascorbic acid (AA) was employed as reference substance. Plain chrysin showed weak antioxidant activity at all tested concentrations. However, all the complexes under evaluation presented dose-dependent antioxidant potential, higher than the pure flavonoid. More specifically, Ni complexes **3** and **4** displayed higher antioxidant activity than cobalt complexes **1** and **2** ($p< 0.001$), plain chrysin ($p< 0.01$) and the control samples $Ni(NO_3)_2{\cdot}6H_2O$, phen and bpy ($p< 0.01$). Co complexes **1** and **2** scavenged DPPH radicals to a greater degree than plain chrysin ($p> 0.05$), $Co(NO_3)_2{\cdot}6H_2O$ ($p> 0.05$) and the corresponding co-ligands ($p< 0.001$). It is worth noting that no significant antioxidant activity was detected in a similar set of experiments utilizing the plain precursors $Ni(NO_3)_2{\cdot}6H_2O$, $Co(NO_3)_2{\cdot}6H_2O$ and co-ligands phen, bpy (Supplementary Information Figure S5).

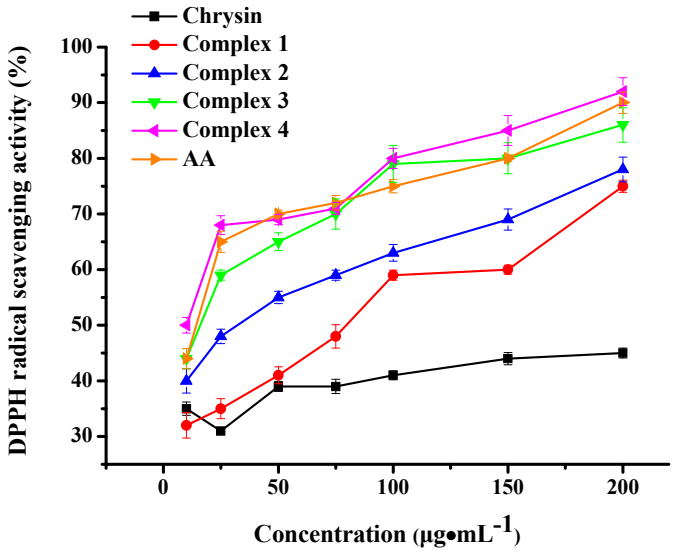


Figure 10. DPPH radical scavenging activity of complexes **1**–**4** and chrysin. AA was employed as standard antioxidant. Data are shown as means ± SEM after three independent measurements.

3. Discussion

The interaction of flavonoids with metal ions has gathered significant attention in the last two decades, in the search of flavonoid-metal complexes with enhanced features and potential drugability. Metal complexation has been shown to strengthen the biological activity of flavonoids and contribute to their stability, solubility, and bioavailability. Although many studies on the synthetic process and physico-chemical characterization of metal-flavonoid complexes are reported in the literature [60,61], yet their structure is scarcely elucidated via X-ray crystallography, mainly because of their negligible solubility and crystallinity.

Our research team has an extended experience in the development of novel crystalline, physico-chemically, structurally, and biologically characterized metallo-flavonoid complexes with a variety of flavonoids and metal ions including lanthanides. Until today, only a few fully characterized via X-ray crystallography metal complexes of chrysin are present in the literature [50–52,62,63], and most of them have been developed by our research team. In this work, a systematic investigation of the experimental conditions led to the development of four crystalline chrysin-based heteroleptic Co(II), Co(III) and Ni(II) complexes with a coordination motif elucidated via spectroscopic, analytical, and X-ray crystallographic techniques.

After careful examination of all reaction parameters, the four complexes were synthesized in alcoholic media employing triethylamine as deprotonating agent. EtOH was chosen as the most appropriate reaction solvent in the cases of complexes **1**, **3**, and **4**, whereas, in the case of complex **2**, MeOH proved to be the most adequate solvent for the formation of stable crystalline material. As observed by our research group in our previous works [50–52], the employment of *N*,*N*-donor chelators, such as bpy and phen, along with the main flavonoid ligand, leads to the formation of stable heteroleptic complexes with exceptional crystallinity and in some cases, remarkable structural differentiation. Interestingly, in this work, the combination of EtOH, triethylamine, and bpy led to the formation of a Co(III) monomeric mononuclear complex **1**, whereas in the case of complex **2**, the combination of MeOH, triethylamine, and phen led to the development of a dimer dinuclear Co(II) complex. The observed differences in the oxidation state of cobalt and structures of these complexes could be attributed to the combined effect of the solvent and *N*,*N*-donor chelator. In the case of complex **1**, it is possible that the lower coordination ability of EtOH for Co(II) [64], compared to MeOH, leaves the metal center more exposed to atmospheric oxygen, resulting in the oxidation of Co(II) $\rightarrow$ Co(III). Moreover, the strong ligand field of the incorporated bpy may stabilize low-spin Co(III) whilst its non-bridging nature and smaller steric demand, compared to that of phen, promote the formation of a monomeric structure. In the case of complex **2**, the combination of MeOH, with the stronger coordination capacity for Co(II), and the co-ligand phen with its rigid, planar structure promoting π-stacking and bridging interactions, facilitated the formation of the final dimeric Co(II) assembly [65,66]. In the case of the Ni(II) complexes, the greater resistance to oxidation of Ni(II) compared to Co(II), may explain the formation of the dimeric Ni(II) complexes **3** and **4**, irrespective of solvent, or type of *N*,*N*-chelator.

As previously reported [67], plain chrysin is a weak DPPH scavenger. Herein, the Ni(II) complexation of chrysin resulted in great enhancement of its radical scavenging activity, that became comparable to that of AA. No significant difference in activity was detected between the bpy and phen-bearing complexes. A comparison to the literature reported Ni(II) complexes revealed that complexes **3** and **4** are better radical scavengers compared to Ni(II)-indomethacin [31], Ni(II)-diflunisal [32], Ni(II)-mefenamato [33], and Ni(II)-naproxen [68] mixed-ligand compounds.

Cobalt complexes **1** and **2** also increased the DPPH scavenging efficiency of chrysin but in a lesser degree compared to Ni(II) complexes **3** and **4**. However, the phen-ligated complex **2** appeared to be a better scavenger than the bpy-ligated complex **1**, a result that is in agreement with documented results on phen or bpy-bearing Co complexes [69]. Herein, the observed scavenging ability is of the same magnitude as recently reported cobalt complexes of non-steroidal anti-inflammatory drugs in the presence or absence of nitrogen-donor heterocyclic ligands [37,38].

The results in this work are in accord with our previous studies on the synthesis and evaluation of novel metal-flavonoid complexes. All complexes exhibited enhanced biological activities such as cytotoxic and ROS generating potential in a series of diverse cancer cell lines [51,70], induction of sister chromatid exchanges, reduction in proliferation rate index and mitotic index values in healthy human lymphocytes and cytotoxic activity against human non-small cell lung carcinoma and lung adenocarcinoma cell lines [50], increased radical scavenging activity [52,71], antioxidant and antibacterial activity [72], and DNA binding potential [73], hence demonstrating the strong effect that metal complexation has on the enhancement of the biological potential of flavonoids.

4. Materials and Methods

A detailed report of the employed equipment, methods and materials is provided in Supplementary Information.

4.1. Synthesis

4.1.1. Synthesis of $[Co(L)(bpy)_2]\cdot(NO_3)_2\cdot 1.5EtOH$ (1)

Ethanolic solutions of $Co(NO_3)_2\cdot 6H_2O$ (0.15 g, 0.5 mmol in 10 mL EtOH) and HL (0.13 g, 0.5 mmol in 10 mL EtOH) were stirred under steady reflux conditions at 60 °C for 90 min. To the occurring bright red clear solution, an ethanolic solution of bpy (0.08 g, 0.5 mmol in 5 mL EtOH) was added under constant stirring. A dark red transparent solution was obtained that was cooled until reaching ambient conditions. To that, triethylamine (55 μL, 0.4 mmol) was added. After 60 min a crimson colored clear solution resulted. To the resulting solution, 1 mL of diethyl ether was gradually added applying the solvent diffusion/layering technique and, after sealing with a rubber septum, the reaction container was refrigerated. This procedure was repeated daily.Twenty days later, dark brown plate-like crystals emerged that were filtrated and vacuum-dried. Yield: 0.06 g (15%). Anal. calcd. for **1**, $[Co(L)(bpy)_2]\cdot(NO_3)_2\cdot 1.5EtOH$ ($C_{38}H_{34}N_6O_{11.5}Co$, Mr: 817.65): C, 55.82; H, 4.19; N, 10.28%. Found: C, 55.73; H, 4.14; N, 10.27%. HR-ESI-MS (positive mode), calcd. for $[Co(L)_2(bpy)]^+$ m/z= 721.1021, found m/z = 721.1011.

4.1.2. Synthesis of $[Co_2(L)_2(phen)_2(MeOH)_2]\cdot(NO_3)_2\cdot 4MeOH$ (2)

Methanolic solutions of $Co(NO_3)_2\cdot 6H_2O$ (0.15 g, 0.5 mmol in 10 mL MeOH) and HL (0.13 g, 0.5 mmol in 10 mL MeOH) were stirred under steady reflux conditions at 60 °C for 90 min. To the bright red clear solution that resulted, a methanolic solution of phen hydrate (0.1 g, 0.5 mmol in 5 mL MeOH) was added under constant stirring. A dark red transparent solution was obtained that was cooled until reaching ambient conditions.To that, triethylamine (70 μL, 0.5 mmol) was added. After 60 min, a crimson colored clear solution resulted. To the resulting solution, diethyl ether was gradually added applying the solvent diffusion/layering technique and, after sealing with a rubber septum, the reaction container was refrigerated. The following day, the reaction vessel was unsealed and left to evaporate slowly at 4 °C. Eight days later, dark red plate like crystalline material emerged that was filtrated and vacuum-dried. Yield: 0.13 g (39%). Anal. calcd. for **2**, $[Co_2(L)_2(phen)_2(MeOH)_2]\cdot(NO_3)_2\cdot 4MeOH$ ($C_{60}H_{58}N_6O_{20}Co_2$, Mr: 1301.01): C, 55.39; H,

4.49; N, 6.46%. Found: C, 55.34; H, 4.44; N, 6.45%. HR-ESI-MS (positive mode), calcd. for $[Co(L)(phen)]^+$ m/z = 492.0520, found m/z = 492.0540.

4.1.3. Synthesis of $[Ni_2(L)_2(bpy)_2(EtOH)_2]\cdot(NO_3)_2\cdot 2EtOH$ (3)

Ethanolic solutions of $Ni(NO_3)_2\cdot 6H_2O$ (0.15 g, 0.5 mmol in 10 mL EtOH) and HL (0.13 g, 0.5 mmol in 10 mL EtOH) were stirred under steady reflux conditions at 60 °C for 90 min. To the bright green clear solution that resulted, an ethanolic solution of bpy (0.08 g, 0.5 mmol in 5 mL EtOH) was added under constant stirring. A green transparent solution was obtained that was cooled until reaching ambient conditions. To that, triethylamine (70 μL, 0.5 mmol) was added. After 60 min, an emerald green homogeneous solution was obtained. To the resulting solution, diethyl ether was gradually added applying the solvent diffusion/layering technique and, after sealing with a rubber septum, the reaction container was refrigerated. Eight days later, green needlelike crystalline precipitate emerged which was filtrated and vacuum-dried.Yield: 0.11 g (35%). Anal. calcd. for **3**, $[Ni_2(L)_2(bpy)_2(EtOH)_2]\cdot(NO_3)_2\cdot 2EtOH$ ($C_{58}H_{58}N_6O_{18}Ni_2$, Mr: 1244.55): C, 55.98; H, 4.70; N, 6.75%. Found: C, 55.98; H, 4.67; N, 6.71%. HR-ESI-MS (positive mode), calcd. for $[Ni(L)(bpy)]^+$ m/z = 467.0542, found m/z = 467.0550.

4.1.4. Synthesis of $[Ni_2(L)_2(phen)_2(EtOH)_2]\cdot(NO_3)_2\cdot 3EtOH$ (4)

Ethanolic solutions of $Ni(NO_3)_2\cdot 6H_2O$ (0.15 g, 0.5 mmol in 10 mL EtOH) and HL (0.13 g, 0.5 mmol in 10 mL EtOH) were stirred under steady reflux conditions at 60 °C for 90 min. To the bright green clear solution that resulted, an ethanolic solution of phen hydrate (0.1 g, 0.5 mmol in 5 mL EtOH) was added under constant stirring. A green homogeneous solution was obtained that was allowed to cool to ambient temperature.To that, triethylamine (70 μL, 0.5 mmol) was added. After 60 min, a deep green transparent solution resulted. To the resulting solution, diethyl ether was gradually added applying the solvent diffusion/layering technique and, after sealing with a rubber septum, the reaction container was refrigerated. Ten days later, green cubic crystalline material emerged that was filtrated and vacuum-dried. Yield: 0.08 g (24%). Anal. calcd. for **4**, $[Ni_2(L)_2(phen)_2(EtOH)_2]\cdot(NO_3)_2\cdot 3EtOH$ ($C_{64}H_{64}N_6O_{19}Ni_2$, Mr: 1338.66): C, 57.42; H, 4.82; N, 6.28%. Found: C, 57.38; H, 4.77; N, 6.27%. HR-ESI-MS (positive mode), calcd. for $[Ni(L)(phen)]^+$ m/z = 491.0542, found m/z = 491.0563.

4.2. X-Ray Crystal Structure Determination

The X-ray monocrystal methodology for the elucidation of the crystal structures of complexes **1–4** is provided in Supplementary Information.

4.3. Antioxidant Activity

The $DPPH^{\cdot}$ protocol was utilized for the *in vitro* estimation of the antioxidant potential of complexes **1–4**, the precursors $Co(NO_3)_2\cdot 6H_2O$ and $Ni(NO_3)_2\cdot 6H_2O$, and the participating ligands chrysin, bpy, and phen, as previously described [71]. Additional information can be found in Supplementary Information.

5. Conclusions

The four novel Co(III)-chrysin-bpy, Co(II)-chrysin-phen, Ni(II)-chrysin-bpy, and Ni(II)-chrysin-phen complexes presented herein demonstrate the effective complexation of flavonoid chrysin with the bioactive Co(II), Co(III) and Ni(II) ions into stable formations. The four complexes were physico-chemically and structurally characterized in solution phase and solid form, indicating a distinct coordination motif around the metal cores with a flavonoid ligand and the ancillary phen and bpy chelators. The *in vitro* biological evalua-

tion revealed notable enhancement of radical scavenging activity after metal complexation, a fact that paves the way for advanced investigation of their pharmacological potential.

Supplementary Materials: The following supporting information can be downloaded at https://www.mdpi.com/article/10.3390/inorganics13070230/s1, Figure S1 HR-ESI-MS spectra of **1**(**A**), **2**(**B**), **3**(**C**), and **4**(**D**); Table S1 Presentation of the examined reaction and (re)crystallization parameters and observations; Table S2 Hydrogen bonds in **1**–**4**; Figure S2 FT-IR spectra of: chrysin (black line), complex **1** (red line), complex **2** (blue line), complex **3** (purple line), complex **4** (green line), bpy (orange line), and phen (brown line); Figure S3 Emission spectra of complexes **1** (**A**), **2** (**B**), **3** (**C**), and **4** (**D**) upon excitation at 540–600 nm; Figure S4 Excitation spectra of complexes **1**–**4** corresponding to the observed fluorescence spectra; Figure S5 Effect of $Ni(NO_3)_2{\cdot}6H_2O$, $Co(NO_3)_2{\cdot}6H_2O$ and co-ligands phen, bpy on DPPH radical scavenging activity. Data were expressed as means ± SEM obtained in three independent experiments.

Author Contributions: Conceptualization, E.H.; methodology, E.H., B.M., D.V., G.Z. and A.G.H.; software, G.Z. and A.G.H.; validation, E.H., B.M., D.V., G.Z. and A.G.H.; formal analysis, E.H., B.M., D.V., G.Z. and A.G.H.; investigation, E.H., B.M., D.V., G.Z. and A.G.H.; resources, E.H.; data curation, E.H., B.M., D.V., G.Z. and A.G.H.; writing—original draft preparation, E.H., B.M., D.V., G.Z. and A.G.H.; writing—review and editing, E.H., B.M., D.V., G.Z., G.L., M.P. and A.G.H.; visualization, E.H., B.M., D.V., G.Z. and A.G.H.; supervision, E.H. and A.G.H.; project administration, E.H.; funding acquisition, E.H. All authors have read and agreed to the published version of the manuscript.

Funding: This research received no external funding.

Institutional Review Board Statement: Not applicable.

Informed Consent Statement: Not applicable.

Data Availability Statement: The raw data supporting the conclusions of this article will be made available by the authors on request. CCDC 2448473 (1), 2448474 (2), 2448475 (3) and 2448476 (4) contain the supplementary crystallographic data for this paper. These data can be obtained free of charge via https://www.ccdc.cam.ac.uk/structures/ (accessed on 3 May 2025) (or from the Cambridge Crystallographic Data Centre, 12 Union Road, Cambridge CB21EZ, UK; fax: (+44) 1223-336-033; or deposit@ccde.cam.ac.uk).

Acknowledgments: E. Halevas acknowledges the Foundation for Education and European Culture (IPEP) founded by Nicos and Lydia Tricha. G. Zahariou gratefully acknowledges helpful discussions with Y. Sanakis on the simulated analysis of the EPR spectra.

Conflicts of Interest: The authors declare no conflicts of interest.

Abbreviations

The following abbreviations are used in this manuscript:

ROS	Reactive Oxygen Species
HL	Chrysin
bpy	2,2′-bipyridine
phen	1,10-phenanthroline
MeOH	Methanol
$Co(NO_3)_2{\cdot}6H_2O$	Cobalt nitrate hexahydrate
$Ni(NO_3)_2{\cdot}6H_2O$	Nickel nitrate hexahydrate
LMCT	Ligand-to-Metal Charge Transfer
AA	Ascorbic Acid
DPPH	2,2-diphenyl-1-picrylhydrazyl
FT-IR	Fourier Transform-Infrared spectroscopy
GC	Gas Chromatography
HR-ESI-MS	High Resolution-ElectroSpray Ionization Mass Spectra
UV-Vis	Ultraviolet-Visible

TGA	Thermogravimetric Analysis
cw	Continuous Wave
EPR	Electron Paramagnetic Resonance
SEM	Standard Error of Mean
ANOVA	Analysis of variance
EtOH	Ethanol
DMA	Dimethylacetamide
DMF	Dimethylformamide
DMSO	Dimethyl sulfoxide

References

1. Chen, S.; Liu, J.; Dong, G.; Zhang, X.; Liu, Y.; Sun, W.; Liu, A. Flavonoids and caffeoylquinic acids in *Chrysanthemum morifolium* Ramat flowers: A potentially rich source of bioactive compounds. *Food Chem.* **2021**, *344*, 128733. [CrossRef]
2. Zhang, T.; Qiu, F.; Chen, L.; Liu, R.; Chang, M.; Wang, X. Identification and in vitro anti-inflammatory activity of different forms of phenolic compounds in *Camellia oleifera* oil. *Food Chem.* **2021**, *344*, 128660. [CrossRef] [PubMed]
3. Wang, N.; Wang, L.; Yang, J.; Wang, Z.; Cheng, L. Quercetin promotes osteogenic differentiation and antioxidant responses of mouse bone mesenchymal stem cells through activation of the AMPK/SIRT1 signaling pathway. *Phytother. Res.* **2021**, *35*, 2639–2650. [CrossRef]
4. Shendge, A.K.; Chaudhuri, D.; Mandal, N. The natural flavones, acacetin and apigenin, induce Cdk-Cyclin mediated G2/M phase arrest and trigger ROS-mediated apoptosis in glioblastoma cells. *Mol. Biol. Rep.* **2021**, *48*, 539–549. [CrossRef] [PubMed]
5. Liu, T.; Xu, J.; Wu, Y.; Li, X.; Ding, D.; Ma, D.; Yao, M.; Wei, W.; Zhang, W.; Wang, S.; et al. Beneficial effects of baicalein on a model of allergic rhinitis. *Acta Pharm.* **2020**, *70*, 35–47. [CrossRef] [PubMed]
6. Wu, Z.; Fan, Q.; Miao, Y.; Tian, E.; Ishfaq, M.; Li, J. Baicalin inhibits inflammation caused by coinfection of *Mycoplasma gallisepticum* and *Escherichia coli* involving IL-17 signaling pathway. *Poult. Sci.* **2020**, *99*, 5472–5480. [CrossRef]
7. Ding, Y.M.; Lin, J.T.; Fang, L.M.; Lou, Z.Q.; Liang, G.N.; Zhang, X.Y.; Li, A.Q.; Zhang, X. The neuroprotective effect of apigenin against OGD/R injury in rat hippocampal neurons. *Pak. J. Pharm. Sci.* **2020**, *33*, 1527–1533.
8. Yue, S.; Xue, N.; Li, H.; Huang, B.; Chen, Z.; Wang, X. Hepatoprotective effect of apigenin against liver injury *via* the non-canonical NF-κB pathway in vivo and in vitro. *Inflammation* **2020**, *43*, 1634–1648. [CrossRef]
9. Stompor-Gorący, M.; Bajek-Bil, A.; Machaczka, M. Chrysin: Perspectives on contemporary status and future possibilities as pro-health agent. *Nutrients* **2021**, *13*, 2038. [CrossRef]
10. Chan, C.W.; Deadman, B.J.; Manley-Harris, M.; Wilkins, A.L.; Alber, D.G.; Harry, E. Analysis of the flavonoid component of bioactive New Zealand mānuka (*Leptospermum scoparium*) honey and the isolation, characterisation and synthesis of an unusual pyrrole. *Food Chem.* **2013**, *141*, 1772–1781. [CrossRef]
11. Wożniak, M.; Mrówczyńska, L.; Kwaśniewska-Sip, P.; Waśkiewicz, A.; Nowak, P.; Ratajczak, I. Effect of the solvent on propolis phenolic profile and its antifungal, antioxidant, and in vitro cytoprotective activity in human erythrocytes under oxidative stress. *Molecules* **2020**, *25*, 4266. [CrossRef]
12. Lopez, A.P.; Galuch, M.B.; Petenuci, M.E.; Oliveira, J.H.; Canesin, E.A.; Schneider, V.V.A.; Visentainer, J.V. Quantification of phenolic compounds in ripe and unripe bitter melons (*Momordica charantia*) and evaluation of the distribution of phenolic compounds in different parts of the fruit by UPLC–MS/MS. *Chem. Pap.* **2020**, *74*, 2613–2625. [CrossRef]
13. Sharma, P.; Kumari, A.; Gulati, A.; Krishnamurthy, S.; Hemalatha, S. Chrysin isolated from *Pyruspashia* fruit ameliorates convulsions in experimental animals. *Nutr. Neurosci.* **2019**, *22*, 569–577. [CrossRef] [PubMed]
14. Xie, Y.; Peng, X. Effect of chrysin on apoptosis of oral squamous cell carcinoma KB cells and its mechanism. *J. Cent. South Univ. Med. Sci.* **2019**, *44*, 522–527.
15. Chen, H.Y.; Jiang, Y.W.; Kuo, C.L.; Day, T.; Chou, Y.C.; Chang, Y.S.; Chung, J.G. Chrysin inhibit human melanoma A375.S2 cell migration and invasion via affecting MAPK signaling and NF-κB signaling pathway in vitro. *Environ. Toxicol.* **2019**, *34*, 434–442. [CrossRef]
16. Ghamkhari, A.; Pouyafar, A.; Salehi, R.; Rahbarghazi, R. Chrysin and docetaxel loaded biodegradable micelle for combination chemotherapy of cancer stem cell. *Pharm. Res.* **2019**, *36*, 165. [CrossRef]
17. Wang, J.N.; Li, X.; Chen, M.F.; Wang, F.Y.; Xiong, X.K.; Chen, X.J.; Yang, M.L.; Huang, J.M. Sensitization of chrysin on the apoptosis induced by cisplatin or camptothecin in hepatoma cell lines (Hep G2). *Chin. Pharm. J.* **2016**, *51*, 2088–2093.
18. Mohos, V.; Fliszár-Nyúl, E.; Schilli, G.; Hetènyi, C.; Lemli, B.; Kunsági-Mátè, S.; Bognár, B.; Poór, M. Interaction of chrysin and its main conjugated metabolites chrysin-7-sulfate and chrysin-7-glucuronide with serum albumin. *Int. J. Mol. Sci.* **2018**, *19*, 4073. [CrossRef]

19. Song, Y.; Wu, W.; Sheng, L.; Jiang, B.; Li, X.; Cai, K. Chrysin ameliorates hepatic steatosis induced by a diet deficient in methionine and choline by inducing the secretion of hepatocyte nuclear factor 4α-dependent very low-density lipoprotein. *J. Biochem. Mol. Toxicol.* **2020**, *34*, e22497. [CrossRef]
20. Li, H.J.; Wu, N.L.; Pu, C.M.; Hsiao, C.Y.; Chang, D.C.; Hung, C.F. Chrysin alleviates imiquimod-induced psoriasis-like skin inflammation and reduces the release of CCL20 and antimicrobial peptides. *Sci. Rep.* **2020**, *10*, 2932. [CrossRef]
21. Bortolotto, V.C.; Araujo, S.M.; Pinheiro, F.C.; Poetini, M.R.; de Paula, M.T.; Meichtry, L.B.; de Almeida, F.P.; Musachio, E.A.S.; Guerra, G.P.; Prigol, M. Modulation of glutamate levels and Na^+, K^+-ATPase activity contributes to the chrysin memory recovery in hypothyroidism mice. *Physiol. Behav.* **2020**, *222*, 112892. [CrossRef] [PubMed]
22. Sadati, S.M.; Gheibi, N.; Ranjbar, S.; Hashemzadehm, M.S. Docking study of flavonoid derivatives as potent inhibitors of influenza H1N1 virus neuraminidase. *Biomed. Rep.* **2019**, *10*, 33–38. [CrossRef] [PubMed]
23. Song, J.H.; Kwon, B.E.; Jang, H.; Kang, H.; Cho, S.; Park, K.; Ko, H.J.; Kim, H. Antiviral activity of chrysin derivatives against Coxsackie virus B3 invitro and in vivo. *Biomol. Ther.* **2015**, *23*, 465–470. [CrossRef]
24. Kwon, M.J.; Shin, H.M.; Perumalsamy, H.; Wang, X.; Ahn, Y.J. Antiviral effects and possible mechanisms of action of constituents from Brazilian propolis and related compounds. *J. Apicult. Res.* **2020**, *59*, 413–425. [CrossRef]
25. Tsuji, P.A.; Walle, T. Cytotoxic effects of the dietary flavones chrysin and apigenin in a normal trout liver cell line. *Chem Biol. Interact.* **2008**, *171*, 37–44. [CrossRef]
26. Harris, G.K.; Qian, Y.; Leonard, S.S.; Sbarra, D.C.; Shi, X. Luteolin and chrysin differentially inhibit cyclooxygenase-2 expression and scavenge reactive oxygen species but similarly inhibit prostaglandin-E_2 formation in raw 264.7 cells. *J. Nutr.* **2006**, *136*, 1517–1521. [CrossRef] [PubMed]
27. Rana, A.C.; Gulliya, B. Chemistry and pharmacology of flavonoids—A review. *Indian J. Pharm. Educ. Res.* **2019**, *53*, 8–20. [CrossRef]
28. Boer, J.L.; Mulrooney, S.B.; Hausinger, R.P. Nickel-dependent metalloenzymes. *Arch. Biochem. Biophys.* **2014**, *544*, 142–152. [CrossRef]
29. Ragsdale, S.W. Nickel-based enzyme systems. *J. Biol. Chem.* **2009**, *284*, 18571–18575. [CrossRef]
30. Zamble, D. Introduction to the biological chemistry of nickel. In *The Biological Chemistry of Nickel*; Zamble, D., Rowińska-Żyrek, M., Kozlowski, H., Eds.; Royal Society of Chemistry: Cambridge, UK, 2017; pp. 1–11.
31. Perontsis, S.; Tialiou, A.; Hatzidimitriou, A.G.; Papadopoulos, A.N.; Psomas, G. Nickel(II)-indomethacin mixed-ligand complexes: Synthesis, characterization, antioxidant activity and interaction with DNA and albumins. *Polyhedron* **2017**, *138*, 258–269. [CrossRef]
32. Tserkezidou, C.; Hatzidimitriou, A.G.; Psomas, G. Nickel(II) complexes of flufenamic acid: Characterization, structure and interaction with DNA and albumins. *Polyhedron* **2016**, *117*, 184–192. [CrossRef]
33. Totta, X.; Papadopoulou, A.A.; Hatzidimitriou, A.G.; Papadopoulos, A.; Psomas, G. Synthesis, structure and biological activity of nickel(II) complexes with mefenamato and nitrogen-donor ligands. *J. Inorg. Biochem.* **2015**, *145*, 79–93. [CrossRef]
34. Gupta, S.K.; Anjana, C.; Sen, N.; Butcher, R.J.; Jasinski, J.P.; Golen, J.A. An unusual hydroxy-substituted mononuclear nickel(II) complex with a tetradentate Schiff base: Synthesis, spectroscopy, electrochemistry, crystallography, DNA binding, and theoretical investigation. *Polyhedron* **2015**, *89*, 219–231. [CrossRef]
35. Kyropoulou, M.; Raptopoulou, C.P.; Psycharis, V.; Psomas, G. Ni(II) complexes withnon-steroidal anti-inflammatory drugdiclofenac: Structure and interaction with DNA and albumins. *Polyhedron* **2013**, *61*, 126–136. [CrossRef]
36. Okamoto, S.; Eltis, L.D. The biological occurrence and trafficking of cobalt. *Metallomics* **2011**, *3*, 963–970. [CrossRef]
37. Tsiliou, S.; Kefala, L.A.; Hatzidimitriou, A.G.; Kessissoglou, D.P.; Perdih, F.; Papadopoulos, A.N.; Turel, I.; Psomas, G. Cobalt(II) complexes with non-steroidal anti-inflammatory drugs and α-diimines. *J. Inorg. Biochem.* **2016**, *160*, 125–139. [CrossRef]
38. Dimiza, F.; Papadopoulos, A.N.; Tangoulis, V.; Psycharis, V.; Raptopoulou, C.P.; Kessissoglou, D.P.; Psomas, G. Biological evaluation of cobalt(II) complexes with non-steroidal anti-inflammatory drug naproxen. *J. Inorg. Biochem.* **2012**, *107*, 54–64. [CrossRef] [PubMed]
39. Thamilarasan, V.; Sengottuvelan, N.; Sudha, A.; Srinivasan, P.; Chakkaravarthi, G. Cobalt(III) complexes as potential anticancer agents: Physicochemical, structural, cytotoxic activity and DNA/protein interactions. *J. Photochem. Photobiol. B Biol.* **2016**, *162*, 558–569. [CrossRef]
40. Ambika, S.; Manojkumar, Y.; Arunachalam, S.; Gowdhami, B.; Kumar, K.; Sundaram, M.; Solomon, R.V.; Venuvanalingam, P.; Akbarsha, M.A.; Sundararaman, M. Biomolecular interaction, anti-cancer and anti-angiogenic properties of cobalt(III) schiffbase complexes. *Sci. Rep.* **2019**, *9*, 2721. [CrossRef]
41. Tsiliou, S.; Kefala, L.A.; Perdih, F.; Turel, I.; Kessissoglou, D.P.; Psomas, G. Cobalt(II) complexes with non-steroidal anti-inflammatory drug tolfenamic acid: Structure and biological evaluation. *Eur. J. Med. Chem.* **2012**, *48*, 132–142. [CrossRef]
42. Pages, B.J.; Ang, D.L.; Wright, E.P.; Aldrich-Wright, J.R. Metal complex interactions with DNA. *Dalton Trans.* **2015**, *44*, 3505–3526. [CrossRef] [PubMed]
43. Bruker Analytical X-Ray Systems, Inc. *Apex2, Version 2 User Manual*; M86-E01078; Bruker Analytical X-Ray Systems, Inc.: Madison, WI, USA, 2006.

44. Siemens Industrial Automation, Inc. *SADABS: Area-Detector Absorption Correction*; Siemens Industrial Automation, Inc.: Madison, WI, USA, 1996.
45. Betteridge, P.W.; Carruthers, J.R.; Cooper, R.I.; Prout, K.; Watkin, D.J. CRYSTALS Version 12: Software for guided crystal structure analysis. *J. Appl. Cryst.* **2003**, *36*, 1487. [CrossRef]
46. Palatinus, L.; Chapuis, G. SUPERFLIP—A computer program for the solution of crystal structures by charge flipping in arbitrary dimensions. *J. Appl. Cryst.* **2007**, *40*, 786–790. [CrossRef]
47. Watkin, D.J.; Prout, C.K.; Pearce, L.J. *CAMERON*; Chemical Crystallography Laboratory: Oxford, UK, 1996.
48. Craig, P.R.; Brothers, P.J.; Clark, G.R.; Wilson, W.R.; Denny, W.A.; Ware, D.C. Anionic carbonato and oxalate cobalt(iii) nitrogen mustard complexes. *Dalton Trans.* **2004**, *2004*, 611–618. [CrossRef]
49. De Meulenaer, J.; Tompa, H. The absorption correction in crystal structure analysis. *Acta Cryst.* **1965**, *19*, 1014. [CrossRef]
50. Halevas, E.; Mitrakas, A.; Mavroidi, B.; Athanasiou, D.; Gkika, P.; Antoniou, K.; Samaras, G.; Lialiaris, E.; Hatzidimitriou, A.; Pantazaki, A.; et al. Structurally characterized copper-chrysin complexes display genotoxic and cytotoxic activity in human cells. *Inorg. Chim. Acta* **2021**, *515*, 120062. [CrossRef]
51. Halevas, E.; Mavroidi, B.; Antonoglou, O.; Hatzidimitriou, A.; Sagnou, M.; Pantazaki, A.A.; Litsardakis, G.; Pelecanou, M. Structurally characterized gallium–chrysin complexes with anticancer potential. *Dalton Trans.* **2020**, *49*, 2734–2746. [CrossRef]
52. Halevas, E.; Mavroidi, B.; Zahariou, G.; Pelecanou, M.; Hatzidimitriou, A.G. Structurally characterized copper complexes of flavonoid naringenin with enhanced radical scavenging activity. *Inorg. Chim. Acta* **2023**, *546*, 121325. [CrossRef]
53. Nakamoto, K. *Infrared and Raman Spectra of Inorganic and Coordination Compounds: Part B: Applications in Coordination, Organometallic, and Bioinorganic Chemistry*, 6th ed.; Wiley Inc.: New York, NY, USA, 2009; pp. 96–98.
54. Boudalis, A.K.; Nastopoulos, V.; Perlepes, S.P.; Raptopoulou, C.P.; Terzis, A. Reactions of 2,2′-bipyridine (bpy) and 1,10-phenanthroline (phen) with yttrium(III) nitrate: Preparation, X-ray crystal structures and spectroscopic characterization of the bis-bpy and bis-phen complexes. *Transit. Metal Chem.* **2001**, *26*, 276–281. [CrossRef]
55. Tan, M.; Zhu, J.; Pan, Y.; Chen, Z.; Liang, H.; Liu, H.; Wang, H. Synthesis, cytotoxic activity, and DNA binding properties of copper(II) complexes with hesperetin, naringenin, and apigenin. *Bioinorg. Chem. Appl.* **2009**, *2009*, 347872. [CrossRef]
56. Tosonian, S.; Ruiz, C.J.; Rios, A.; Frias, E.; Eichler, J.F. Synthesis, characterization, and stability of iron(III) complex ions possessing phenanthroline-based ligands. *Open J. Inorg. Chem.* **2013**, *3*, 7–13. [CrossRef] [PubMed]
57. Duval, C. *Inorganic Thermogravimetric Analysis*, 2nd ed.; Elsevier Publishing Co.: Amsterdam, The Netherlands, 1963; pp. 416–420.
58. Stoll, S.; Schweiger, A. EasySpin, a comprehensive software package for spectral simulation and analysis in EPR. *J. Magn. Reson.* **2006**, *178*, 42–55. [CrossRef] [PubMed]
59. Kedare, S.B.; Singh, R.P. Genesis and development of DPPH method of antioxidant assay. *J. Food Sci. Technol.* **2011**, *48*, 412–422. [CrossRef] [PubMed]
60. Khater, M.; Ravishankar, D.; Greco, F.; Osborn, H.M. Metal complexes of flavonoids: Their synthesis, characterization and enhanced antioxidant and anticancer activities. *Future Med. Chem.* **2019**, *11*, 2845–2867. [CrossRef]
61. Kasprzak, M.M.; Erxleben, A.; Ochocki, J. Properties and applications of flavonoid metal complexes. *RSC Adv.* **2015**, *5*, 45853–45877. [CrossRef]
62. Matsia, S.; Lazopoulos, G.; Hatzidimitriou, A.; Reimann, M.K.; Pöttgen, R.; Salifoglou, A. Chemical reactivity profile of rare earth metal ions with flavonoids. From structural speciation to magneto-optical properties. *Polyhedron* **2023**, *230*, 116231. [CrossRef]
63. Matsia, S.; Tsave, O.; Hatzidimitriou, A.; Salifoglou, A. Chromium flavonoid complexation in an antioxidant capacity role. *Int. J. Mol. Sci.* **2022**, *23*, 7171. [CrossRef]
64. Payehghadr, M.; Hashemi, S.E. Solvent effect on complexation reactions. *J. Incl. Phenom. Macrocycl. Chem.* **2017**, *89*, 253–271. [CrossRef]
65. Liu, J.; Lorraine, S.C.; Dolinar, B.S.; Hoover, J.M. Aerobic oxidation reactivity of well-defined cobalt(II) and cobalt(III) aminophenol complexes. *Inorg. Chem.* **2022**, *61*, 6008–6016. [CrossRef]
66. Bencini, A.; Lippolis, V. 1,10-Phenanthroline: A versatile building block for the construction of ligands for various purposes. *Coord. Chem. Rev.* **2010**, *254*, 2096–2180. [CrossRef]
67. Uivarosi, V.; Munteanu, A.C. Flavonoid complexes as promising anticancer metallodrugs. In *Flavonoids—From Biosynthesis to Human Health*; Justino, G.C., Ed.; IntechOpen: London, UK, 2017; pp. 305–334.
68. Totta, X.; Hatzidimitriou, A.G.; Papadopoulos, A.N.; Psomas, G. Nickel(ii)–naproxen mixed-ligand complexes: Synthesis, structure, antioxidant activity and interaction with albumins and calf-thymus DNA. *New J. Chem.* **2017**, *41*, 4478–4492. [CrossRef]
69. Festus, C.; Okafor, S.N.; Ekennia, A.C. Heteroleptic metal complexes of a pyrimidinyl based schiff base ligand incorporating 2,2′-bipyridine moiety: Synthesis, characterization, and biological studies. *Front. Chem.* **2019**, *7*, 862. [CrossRef] [PubMed]
70. Halevas, E.; Mavroidi, B.; Kaplanis, M.; Hatzidimitriou, A.G.; Moschona, A.; Litsardakis, G.; Pelecanou, M. Hydrophilic bis-MPA hyperbranched dendritic scaffolds as nanocarriers of a fully characterized flavonoid morin-Zn(II) complex for anticancer applications. *J. Inorg. Biochem.* **2022**, *232*, 111832. [CrossRef]

71. Halevas, E.; Mavroidi, B.; Pelecanou, M.; Hatzidimitriou, A.G. Structurally characterized zinc complexes of flavonoids chrysin and quercetin with antioxidant potential. *Inorg. Chim. Acta* **2021**, *523*, 120407. [CrossRef]
72. Halevas, E.; Matsia, S.; Hatzidimitriou, A.; Geromichalou, E.; Papadopoulos, T.A.; Katsipis, G.; Pantazaki, A.; Litsardakis, G.; Salifoglou, A. A unique ternary Ce(III)-quercetin-phenanthroline assembly with antioxidant and anti-inflammatory properties. *J. Inorg. Biochem.* **2022**, *235*, 111947. [CrossRef]
73. Halevas, E.; Pekou, A.; Papi, R.; Mavroidi, B.; Hatzidimitriou, A.G.; Zahariou, G.; Litsardakis, G.; Sagnou, M.; Pelecanou, M.; Pantazaki, A.A. Synthesis, physicochemical characterization and biological properties of two novel Cu(II) complexes based on natural products curcumin and quercetin. *J. Inorg. Biochem.* **2020**, *208*, 111083. [CrossRef]

Disclaimer/Publisher's Note: The statements, opinions and data contained in all publications are solely those of the individual author(s) and contributor(s) and not of MDPI and/or the editor(s). MDPI and/or the editor(s) disclaim responsibility for any injury to people or property resulting from any ideas, methods, instructions or products referred to in the content.